



# A Linear Relation between the Color Stretch $s_{BV}$ and the Rising Color Slope $s_0^*(B - V)$ of Type Ia Supernovae

Ping Chen<sup>1,2,3</sup> , Subo Dong<sup>1</sup> , Chris Ashall<sup>4</sup> , S. Benetti<sup>5</sup>, D. Bersier<sup>6</sup> , S. Bose<sup>7,8</sup> , Joseph Brimacombe<sup>9</sup>, Thomas G. Brink<sup>10</sup> , David A. H. Buckley<sup>11</sup>, Enrico Cappellaro<sup>5</sup> , Grant W. Christie<sup>12</sup>, N. Elias-Rosa<sup>13,14</sup> , Alexei V. Filippenko<sup>10</sup> , Mariusz Gromadzki<sup>15</sup> , Thomas W.-S. Holoien<sup>16,34</sup> , Shaoming Hu<sup>17</sup>, C. S. Kochanek<sup>7,8</sup> , Robert Koff<sup>18</sup>, Juna A. Kollmeier<sup>19</sup>, P. Lundqvist<sup>20</sup> , S. Mattila<sup>21</sup>, Peter A. Milne<sup>22</sup> , J. A. Muñoz<sup>23,24</sup> , Robert Mutel<sup>25</sup> , Tim Natusch<sup>26</sup>, Joel Nicolas<sup>27</sup>, A. Pastorello<sup>5</sup> , Simon Prentice<sup>28</sup> , J. L. Prieto<sup>29,30</sup> , Tyler Roth<sup>25</sup>, B. J. Shappee<sup>4</sup> , Geoffrey Stone<sup>31</sup>, K. Z. Stanek<sup>7,8</sup>, M. D. Stritzinger<sup>32</sup> , Todd A. Thompson<sup>7,8</sup> , Lina Tomasella<sup>5</sup> , and Steven Villanueva<sup>33,35</sup>

<sup>1</sup> Kavli Institute for Astronomy and Astrophysics, Peking University, Yi He Yuan Road 5, Hai Dian District, Beijing 100871, People's Republic of China  
[chenp1220@pku.edu.cn](mailto:chenp1220@pku.edu.cn)

<sup>2</sup> Department of Astronomy, School of Physics, Peking University, Yi He Yuan Road 5, Hai Dian District, Beijing 100871, People's Republic of China

<sup>3</sup> Department of Particle Physics and Astrophysics, Weizmann Institute of Science, Rehovot 7610001, Israel

<sup>4</sup> Institute for Astronomy, University of Hawaii at Manoa, 2680 Woodlawn Drive, Honolulu, HI 96822, USA

<sup>5</sup> INAF—Osservatorio Astronomico di Padova, Vicolo dell'Osservatorio 5, I-35122 Padova, Italy

<sup>6</sup> Astrophysics Research Institute, Liverpool John Moores University, 146 Brownlow Hill, Liverpool L3 5RF, UK

<sup>7</sup> Department of Astronomy, The Ohio State University, 140 West 18th Avenue, Columbus, OH 43210, USA

<sup>8</sup> Center for Cosmology and Astroparticle Physics, The Ohio State University, 191 W. Woodruff Avenue, Columbus, OH 43210, USA

<sup>9</sup> Coral Towers Observatory, Queensland, Australia

<sup>10</sup> Department of Astronomy, University of California, Berkeley, CA 94720-3411, USA

<sup>11</sup> South African Astronomical Observatory, P.O. Box 9, Observatory 7935, Cape Town, South Africa

<sup>12</sup> Auckland Observatory, Auckland, New Zealand

<sup>13</sup> INAF Osservatorio Astronomico di Padova, Vicolo dell'Osservatorio 5, I-35122 Padova, Italy

<sup>14</sup> Institute of Space Sciences (ICE, CSIC), Campus UAB, Carrer de Can Magrans s/n, E-08193 Barcelona, Spain

<sup>15</sup> Astronomical Observatory, University of Warsaw, Al. Ujazdowskie 4, 00-478 Warszawa, Poland

<sup>16</sup> The Observatories of the Carnegie Institution for Science, 813 Santa Barbara Street, Pasadena, CA 91101, USA

<sup>17</sup> Shandong Key Laboratory of Optical Astronomy and Solar-Terrestrial Environment, Institute of Space Sciences, School of Space Science and Physics, Shandong University, Weihai, Shandong, 264209, People's Republic of China

<sup>18</sup> Antelope Hills Observatory, 980 Antelope Drive West, Bennett, CO 80102, USA

<sup>19</sup> Observatories of the Carnegie Institution for Science, 813 Santa Barbara Street, Pasadena, CA 91101, USA

<sup>20</sup> The Oskar Klein Centre, Department of Astronomy, Stockholm University, AlbaNova, SE-10691, Stockholm, Sweden

<sup>21</sup> Tuorla Observatory, Department of Physics and Astronomy, University of Turku, FI-20014 Turku, Finland

<sup>22</sup> University of Arizona, Steward Observatory, 933 North Cherry Avenue, Tucson, AZ 85721, USA

<sup>23</sup> Departamento de Astronomía y Astrofísica, Universidad de Valencia, E-46100 Burjassot, Valencia, Spain

<sup>24</sup> Observatorio Astronómico, Universidad de Valencia, E-46980 Paterna, Valencia, Spain

<sup>25</sup> Department of Physics and Astronomy, University of Iowa, Iowa City, IA 52242, USA

<sup>26</sup> Institute for Radio Astronomy and Space Research (IRASR), AUT University, Auckland, New Zealand

<sup>27</sup> Io Variables-CCD group, 364 chemin de Notre Dame, F-06220 Vallauris, France

<sup>28</sup> School of Physics, Trinity College Dublin, The University of Dublin, Dublin 2, Ireland

<sup>29</sup> Núcleo de Astronomía de la Facultad de Ingeniería y Ciencias, Universidad Diego Portales, Avenida Ejército 441, Santiago, Chile

<sup>30</sup> Millennium Institute of Astrophysics, Santiago, Chile

<sup>31</sup> CBA Sierras, 44325 Alder Heights Road, Auberry, CA 93602, USA

<sup>32</sup> Department of Physics and Astronomy, Aarhus University, Ny Munkegade 120, DK-8000 Aarhus C, Denmark

<sup>33</sup> Massachusetts Institute of Technology, Cambridge, MA 02139, USA

Received 2021 December 24; revised 2023 March 8; accepted 2023 March 9; published 2023 April 5

## Abstract

Using data from the Complete Nearby (redshift  $z_{\text{host}} < 0.02$ ) sample of Type Ia Supernovae (CNIa0.02), we find a linear relation between two parameters derived from the  $B - V$  color curves of Type Ia supernovae: the *color stretch*  $s_{BV}$  and the rising color slope  $s_0^*(B - V)$  after the peak, and this relation applies to the full range of  $s_{BV}$ . The  $s_{BV}$  parameter is known to be tightly correlated with the peak luminosity, especially for *fast decliners* (dim Type Ia supernovae), and the luminosity correlation with  $s_{BV}$  is markedly better than with the classic light-curve width parameters such as  $\Delta m_{15}(B)$ . Thus, our new linear relation can be used to infer peak luminosity from  $s_0^*$ . Unlike  $s_{BV}$  (or  $\Delta m_{15}(B)$ ), the measurement of  $s_0^*(B - V)$  does not rely on a well-determined time of light-curve peak or color maximum, making it less demanding on the light-curve coverage than past approaches.

<sup>34</sup> NHFP Einstein Fellow.

<sup>35</sup> Pappalardo Fellow.



*Unified Astronomy Thesaurus concepts:* Type Ia supernovae (1728); Supernovae (1668); Time series analysis (1916); Light curves (918)

*Supporting material:* figure set, machine-readable table

## 1. Introduction

As a supernova (SN) population, Type Ia supernovae (SNe Ia) show remarkable regularities in observed properties; in particular, their light curves follow a tight relation between peak luminosity and the decline rate, which is commonly referred to as the width–luminosity relation (WLR; see Phillips & Burns 2017 for a review). The empirical WLR extends from the most luminous SN 1991T-like SNe Ia (Filippenko et al. 1992b; Phillips et al. 1992; Ruiz-Lapuente et al. 1992) to the least luminous SN 1991bg-like SNe Ia (Filippenko et al. 1992a; Leibundgut et al. 1993; Turatto et al. 1996). The WLR not only offers important clues to understanding the physics of the SN Ia population, but also enables using SNe Ia as important cosmological distance indicators.

Pskovskii (1977, 1984) suggested the existence of the WLR for SNe Ia by using a post-peak slope parameter,  $\beta$ , to measure the light-curve decline rate. Its validity was called into question by some researchers owing to concerns over host-galaxy contamination to the SN flux measurements obtained with photographic plates (see, e.g., Boisseau & Wheeler 1991). Phillips (1993) established the WLR by using well-sampled light curves of nearby SNe Ia observed with charge-coupled devices and introduced the now-classic width parameter  $\Delta m_{15}(B)$ , which is the  $B$ -band magnitude difference between the magnitude at the time of peak brightness ( $t_{\text{peak}}(B)$ ) and 15 days afterward. Later, other, similar width parameterizations such as the *stretch*  $s$  were introduced (Perlmutter et al. 1997), and there were also variants like  $x_1$  in SALT2 (Guy et al. 2007) or  $\Delta$  (Riess et al. 1996; Jha et al. 2007).

In order to accurately derive  $\Delta m_{15}(B)$  directly from the light curve, good photometric coverage before  $t_{\text{peak}}(B)$  to at least 15 days after  $t_{\text{peak}}(B)$  is required. Since the light curves evolve slowly over the peak (varying by only  $\sim 0.1$  mag in 1 week), an accurate peak-time determination is challenging if the light curve is not densely sampled around the peak. In practice, various template-fitting methods are often employed to derive  $\Delta m_{15}(B)$  using well-sampled light-curve templates with known  $\Delta m_{15}(B)$  (see, e.g., Hamuy et al. 1995, 1996; Prieto et al. 2006; Burns et al. 2011).

For low-luminosity, fast-declining SNe Ia,  $\Delta m_{15}(B)$  is found to be a poor width discriminator, and the WLR using  $\Delta m_{15}(B)$  shows large scatter for  $\Delta m_{15}(B) \gtrsim 1.7$  mag (see, e.g., Burns et al. 2014; Gall et al. 2018). Similarly, the stretch method fails for fast decliners (see, e.g., Phillips & Burns 2017). From studying high-quality  $B - V$  color curves of SNe Ia observed by the Carnegie Supernova Project (CSP), Burns et al. (2014) found that fast-declining SNe Ia reach their reddest  $B - V$  color earlier than those with slower decline rates. To better characterize this, Burns et al. (2014) introduced the *color-stretch* parameter,  $s_{BV}$ , which is a dimensionless stretch-like parameter defined as  $s_{BV} = t_{\text{max}}(B - V)/(30 \text{ days})$ , where  $t_{\text{max}}(B - V)$  is time to the maximum (reddest)  $B - V$  color with reference to the  $B$ -band maximum. Since the  $B - V$  color quickly declines after reaching maximum,  $t_{\text{max}}(B - V)$  corresponds to a sharp *break* in the  $B - V$  color curve (see Figure 1 for examples). Using  $s_{BV}$  as a proxy for decline rate (instead of  $\Delta m_{15}(B)$ ), the scatter in the WLR significantly

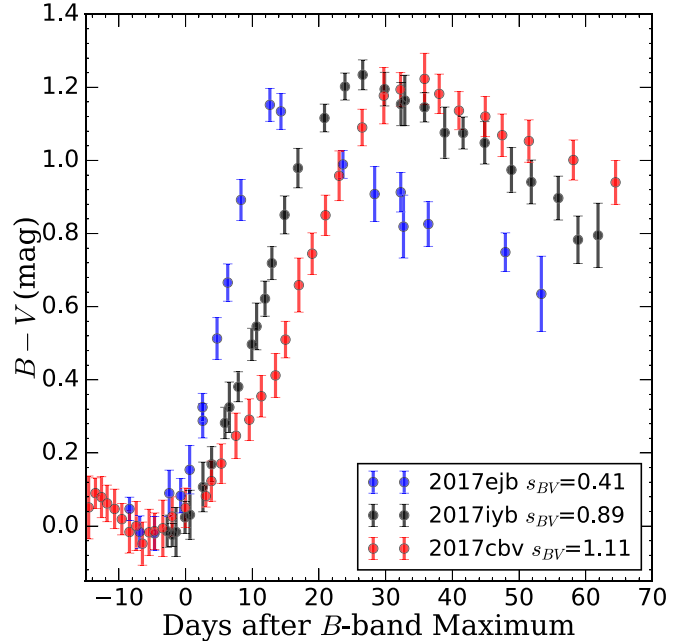


**Figure 1.**  $B - V$  color curves of SNe Ia 2017ejb, 2017iyb, and 2017cbv. The data for SN 2017ejb is shifted downward by 0.25 mag to match the local minimum of  $B - V$  color,  $(B - V)_{\text{min}}$ , of the other two SNe. After the  $B$ -band peak, the  $B - V$  color curves have the typical evolution of first rising and then declining. The three SNe reach their maximum  $B - V$  colors at different times, which correspond to different  $s_{BV}$  values (see text for how they are measured). The rising slope seems to be correlated with the time of the maximum  $B - V$  color.

reduces at the low-luminosity end, and SNe Ia over the full range of luminosity lie on a tight and continuous correlation (Burns et al. 2018). Moreover, Ashall et al. (2020) found that combining  $s_{BV}$  with the time difference between  $B$ -band and  $i$ -band maxima is useful to discriminate between SN Ia subtypes.

Reducing the scatter in the WLR using  $s_{BV}$  not only has important implications for using SNe Ia as distance indicators, but also sheds new insight into the physics of WLRs. Wygoda et al. (2019) found that  $t_{\text{max}}(B - V)$  corresponds to an abrupt change in the mean opacities due to ionization-state transitions of  $^{56}\text{Fe}$  and  $^{56}\text{Co}$  in the ejecta, while the timescale to reach the color maximum is determined by the ejecta  $^{56}\text{Ni}$  column density, which sets the recombination time of Fe/Co ions.

To derive  $s_{BV}$  from light curves, it is required to measure not only  $t_{\text{max}}(B - V)$ , but also, like  $\Delta m_{15}(B)$ , a precise estimate of  $t_{\text{peak}}(B)$ . In this work, we report the finding of a linear relation between  $s_{BV}$  and the rising linear slope of the  $B - V$  color curve of SNe Ia, which is defined as  $s_0^*(B - V)$  by us, using the CNIa0.02 sample (Chen et al. 2022). As a proxy for light-curve width and in turn, the peak luminosity via the WLR,  $s_0^*(B - V)$  has the merit of being less demanding on light-curve coverage.

It is noteworthy that the Color-MAGNitude Intercept Calibration (CMAGIC) method developed by Wang et al. (2006) and Conley et al. (2006) shares the same advantage of being less demanding on light-curve coverage when using the WLR. The CMAGIC method also exploited the color curves of SNe Ia, and it was built on the empirical linear relation between

**Table 1**  
Light-curve Parameters of SNe Ia in the CNIa.02 Sample

SN	$t_{\text{peak}}(B)$ (MJD)	$\Delta m_{15}(B)$ (mag)	$s_0$	$s_1$	$s_{BV}$	$s_0^*$
2016bfu	$57469.7 \pm 0.6$	$1.81 \pm 0.09$	$0.109 \pm 0.019$	$-0.0129 \pm 0.0053$	$0.49 \pm 0.09$	$0.076 \pm 0.012$
2016blc	$57489.8 \pm 1.1$	$0.99 \pm 0.13$	$0.050 \pm 0.005$	$-0.0099 \pm 0.0014$	$1.08 \pm 0.09$	$0.048 \pm 0.003$
2016fff	$57630.0 \pm 0.2$	$1.81 \pm 0.06$	$0.082 \pm 0.009$	$-0.0119 \pm 0.0039$	$0.67 \pm 0.09$	$0.076 \pm 0.002$
2016fej	$57635.5 \pm 0.7$	$0.89 \pm 0.08$	$0.049 \pm 0.002$	$-0.0125 \pm 0.0007$	$1.07 \pm 0.04$	$0.049 \pm 0.003$
2016gtr	$57667.1 \pm 0.9$	$0.94 \pm 0.11$	$0.045 \pm 0.005$	$-0.0204 \pm 0.0068$	$1.18 \pm 0.07$	$0.043 \pm 0.001$

(This table is available in its entirety in machine-readable form.)

color and magnitude (e.g.,  $B - V$  versus  $B$  magnitude) during post-peak phases whose slope has a nearly constant value over a wide range of light-curve widths (Wang et al. 2003).

## 2. Light-curve Analysis

Here, we analyze the  $B$ - and  $V$ -band light curves presented by Chen et al. (2022). We include SNe Ia ranging from the most luminous end (i.e., SN 1991T-like) to the least luminous end (i.e., SN 1991bg-like) in the analysis, while we exclude five objects that do not belong to the complete sample of CNIa.02 (see Appendix D of Chen et al. 2022 for details regarding those excluded objects). In order to obtain accurate  $s_{BV}$  measurements, we need to reliably infer the time of the  $B$ -band peak,  $t_{\text{peak}}(B)$ , and the time of maximum  $B - V$  color,  $t_{\text{max}}(B - V)$ . We discuss below how we select the SNe used in the analysis.

First, the  $B$ -band light curves need to have coverage around the peak to infer  $t_{\text{peak}}(B)$ . We adopt the criterion of having at least 3 epochs within 6 days of the peak and at least 4 points within 10 days of the peak. Throughout the paper (unless otherwise specified),  $t_{\text{peak}}(B)$  is used as the reference time. It is obtained with the Gaussian process method if pre-peak data are available; otherwise, it is derived from template fitting using SNooPy (Burns et al. 2011). We list the derived  $t_{\text{peak}}(B)$  and  $\Delta m_{15}(B)$  values in Table 1.

Next, we analyze the  $B - V$  color curves for all remaining SNe to infer  $s_{BV}$ , and the SNe without data late enough to derive  $t_{\text{max}}(B - V)$  are excluded from the analysis. To obtain reliable  $s_{BV}$  values, we impose the following selection criteria: (1) the  $B - V$  color curve needs to have at least 4 data points covering no less than half of the time range between  $t_{\text{peak}}(B)$  and  $t_{\text{max}}(B - V)$ ; and (2) after  $t_{\text{max}}(B - V)$ , there need to be at least 2 data points spanning more than 5 days, and the last data point needs to be at least  $\sim 10$  days after  $t_{\text{max}}(B - V)$ . The phase of the  $B - V$  color curve is corrected for time dilation. Since all targets have low redshifts, the  $K$ -correction is negligible for our analysis and thus is not applied.

In Figure 1, we show the  $B - V$  color curves of three SNe Ia with  $s_{BV} = 0.41, 0.89,$  and  $1.11$ , respectively. After  $t_{\text{peak}}(B)$ , the  $B - V$  color curve soon enters a linear rise phase (hence, becoming redder), followed by a linear decline (becoming bluer) after  $t_{\text{max}}(B - V)$ . The rising slope and  $t_{\text{max}}(B - V) - t_{\text{peak}}(B)$  seem to correlate with each other. It has been recognized previously that fast decliners tend to have faster post-peak  $B - V$  color evolution compared to those with higher luminosity (see, e.g., Hoefflich et al. 2017). Here for the first time we measure the relevant light-curve parameters to quantitatively study the observed correlation. In the following, we describe how we measure the parameters from the color curves.

We fit the time evolution of the  $B - V$  color since the onset of the post-peak linear rise phase based on Equation (2) of Burns et al. (2014). The model has the form

$$y(t) = \frac{1}{2}(s_0 + s_1)t + \frac{\tau}{2}(s_1 - s_0) \ln \left[ \cosh \left( \frac{t - t_h}{\tau} \right) \right] + c, \quad (1)$$

where  $t$  is the rest-frame time relative to  $t_{\text{peak}}(B)$ ,  $s_0$  and  $s_1$ , respectively, characterize the rising and declining slopes,  $\tau$  is the transition timescale indicating how fast the color curve changes from the rising to the declining slope, and  $t_h$  is the time when the derivative of  $y(t)$  is equal to the averaged value of the initial and final slopes (i.e.,  $y'(t_h) = (s_0 + s_1)/2$ ). We drop the last polynomial term on the right-hand side in Equation (2) of Burns et al. (2014), since that term is used for modeling the color curve prior to the onset of the linear rise phase. In addition, we correct a typographical error in the first term (correcting  $(s_0 - s_1)/2$  of Burns et al. 2014 to  $(s_0 + s_1)t/2$ ). Note that in this model, the rising and declining sides are not strictly linear with time, and  $s_0$  and  $s_1$  (respectively) are only supposed to be close to the first derivatives for most parts of the two sides. We illustrate the example of SN 2017cbv in Figure 2, in which the best-fit model is shown with a red line. The time of the maximum  $B - V$  color where  $y'(t_{\text{max}}(B - V)) = 0$ , as indicated by the vertical line in Figure 2, is<sup>36</sup>

$$t_{\text{max}}(B - V) = \frac{\tau}{2} \ln \left( -\frac{s_0}{s_1} \right) + t_h. \quad (2)$$

We note that the phase when the linear rise starts,  $t_s$ , is correlated with  $t_{\text{max}}(B - V)$ . SNe Ia with higher  $s_{BV}$  enter the linear phase at a later time. We adopt an empirical estimate of  $t_s = 0.3 t_{\text{max}}(B - V) - 2$  days after  $t_{\text{peak}}(B)$  as the start phase for our fitting. The adopted end phase for fitting is 90 days after  $t_{\text{peak}}(B)$ . Since  $t_{\text{max}}(B - V)$  is needed to derive the phase range used for the fit, we iteratively determine this phase range with an initial range of [5, 90] days.

We fit the  $B - V$  color curves using the Markov Chain Monte Carlo (MCMC) method to get the best-fit values of all the parameters in Equation (1). Equation (2) is used to determine  $t_{\text{max}}(B - V)$  and then  $s_{BV} = t_{\text{max}}(B - V)/30$ . The derived  $s_{BV}$ ,  $s_0$ , and  $s_1$  parameters for 86 SNe Ia with their uncertainties are given in Table 1.

<sup>36</sup> Note that  $t_h$  was inaccurately regarded as the time of  $B - V$  maximum by Burns et al. (2014) (C. Burns 2023, private communications).

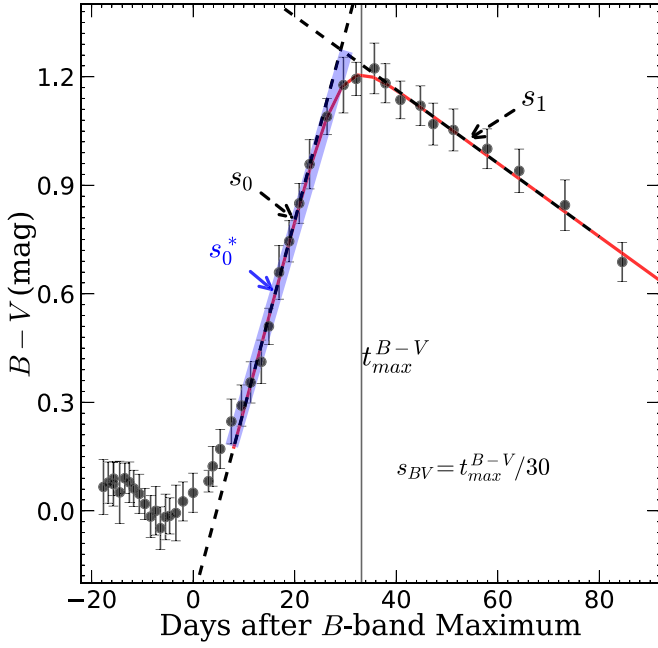


**Figure 2.**  $B - V$  color curve of SN 2017cbv with best-fit results shown as an example of the procedure described in this paper. The observed data are shown as black dots and the best-fit model with Equation (1) is shown in red. The black dashed lines indicate the rising slope  $s_0$  and declining slope  $s_1$  from Equation (1). The vertical black line marks the time of the reddest  $B - V$  color. The direct linear fit to get the rising slope  $s_0^*(B - V)$  is shown as the blue line. The extent of the blue line indicates the range of the linear region defined by  $[t_s, t_e] = [0.3 t_{\max}(B - V) - 2, 0.9 t_{\max}(B - V)]$ . (The complete figure set with a simplified version of the plots for all 86 objects used to derive the linear relation is available in the online journal.)

(The complete figure set (86 images) is available.)

In the above MCMC fitting of the  $B - V$  color curve, we applied uniform priors for all parameters. We found that the best-fit value of  $\tau$  is highly sensitive to its prior. Our work was initially motivated by the apparent correlation between  $s_{BV}$  and  $s_0$ . However, after further investigation, we found that  $s_0$  is also correlated with  $\tau$ ; therefore, the best-fit value of  $s_0$  from the MCMC fitting is affected by the prior that we placed on  $\tau$ . The reason for the effect of  $\tau$  on  $s_0$  can be understood by examining the time derivative of Equation (1),

$$y'(t) = \frac{s_0 + s_1}{2} + \frac{s_1 - s_0}{2} \tanh\left(\frac{t - t_h}{\tau}\right). \quad (3)$$

Clearly the deviation of  $y'(t)$  from a constant (i.e., as followed from a linear model with respect to  $t$ ) in the rising part of the model depends on  $\tau$ . In practice, the derived values of  $\tau$  often have relatively large uncertainties, and they also correlate with  $s_{BV}$ , making it difficult to establish a clear-cut correlation between  $s_0$  and  $s_{BV}$ .

Instead of using  $s_0$  defined in Equation (1), we measure the rising slope by directly fitting a linear model  $y(t) = s_0^* t + c^*$  to the rising part of the color curve. To do so, we need to determine a phase range  $[t_s, t_e]$  during which the color curve is well characterized by a linear model. As can be seen from Figure 1, both the beginning and end phases of the linear phase seem to be correlated with the time of maximum  $B - V$  color. Therefore, the values of  $t_s$  and  $t_e$  depend on  $t_{\max}(B - V)$ . After some experimentation, we find that the range defined with  $t_s = 0.3 t_{\max}(B - V) - 2$  and

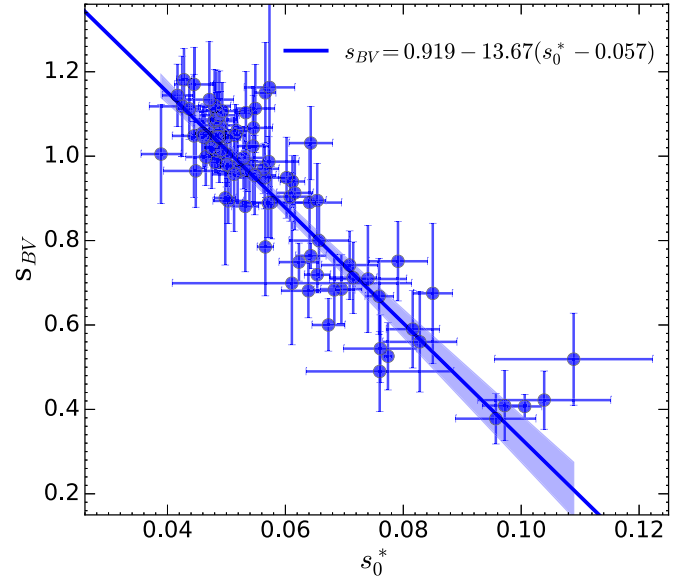


**Figure 3.** Correlation between the color-stretch parameter,  $s_{BV}$ , and the rising color slope,  $s_0^*$ , of the  $B - V$  color. All of the measurements for 86 SNe Ia in Table 1 are shown here. The blue line indicates the best linear fit and the shaded range indicates the 95% confidence region for the fit.

$t_e = 0.9 t_{\max}(B - V)$  can be well characterized by a linear model for SNe Ia with a broad range of  $s_{BV}$ . The best-fit linear model within such a range is shown as a blue line in Figure 2. We exclude from the analysis SNe Ia with fewer than 3 points in the  $B - V$  color curve within  $[t_s, t_e]$ . In the end, 86 SNe Ia meet all of the above criteria. The directly measured rising color slope parameters,  $s_0^*$ , are provided in Table 1. By comparing the values of  $s_0$  and  $s_0^*$ , we find that  $s_0$  tends to be larger than  $s_0^*$ .

### 3. Results

As shown in Figure 3, we clearly see that  $s_0^*$  and  $s_{BV}$  are linearly correlated; the linear correlation coefficient is  $r = -0.90$ , which is highly significant. We perform a linear fit with the Orthogonal Distance Regression method (Boggs et al. 1987) implemented in the Python package Kapteyn (Terlouw & Vogelaar 2016). The best-fit linear model between  $s_0^*$  and  $s_{BV}$  accounting for uncertainties yields

$$s_{BV} = 0.919(0.008) - 13.67(0.61) \times (s_0^* - 0.057). \quad (4)$$

The uncertainties given in the parentheses are obtained by scaling the measurement errors of  $s_0^*$  and  $s_{BV}$  to have  $\chi^2/\text{dof} = 1$ , where ‘‘dof’’ is the number of degrees of freedom. The residuals to this best-fit linear model have a scatter of 0.093 in  $s_{BV}$ , comparable with the median  $s_{BV}$  measurement uncertainty of 0.082. The uncertainties in the  $s_0^*$  inference also affect how tight the derived relation is. CNIa0.02 light curves were observed with multiple instruments having various natural-filter systems, which may also introduce systematic differences in the  $B - V$  color curves that contribute to the scatter seen here. This linear relation between  $s_{BV}$  and  $s_0^*$  suggests that  $s_0^*$  can be used to infer  $s_{BV}$ .

As shown in the left panel of Figure 4, we compare  $s_0^*(B - V)$  with  $\Delta m_{15}(B)$  using our sample. Similar to the well-known trends (Burns et al. 2014) when comparing  $s_{BV}$  and  $\Delta m_{15}(B)$  (right panel of Figure 4), there is a linear correlation

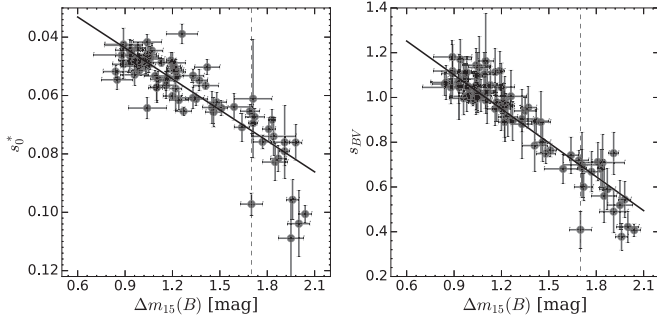


**Figure 4.** Comparisons of  $s_0^*(B - V)$  (left) and  $s_{BV}$  (right) with respect to  $\Delta m_{15}(B)$ . For SNe Ia with  $\Delta m_{15}(B) < 1.7$  mag (vertical dashed lines), both  $s_0^*$  and  $s_{BV}$  are linearly correlated with  $\Delta m_{15}(B)$  (the black lines in both panels), whereas there is a large scatter for fast decliners with  $\Delta m_{15}(B) > 1.7$  mag.

for SNe Ia with  $\Delta m_{15}(B) < 1.7$  mag; however, for those with  $\Delta m_{15}(B) > 1.7$  mag, there is large scatter.

The inference of  $s_0^*$  has comparative merit over  $s_{BV}$  or  $\Delta m_{15}(B)$  in the data-coverage requirements. Measuring  $s_{BV}$  depends on determining two critical timing parameters,  $t_{\text{peak}}(B)$  and  $t_{\text{max}}(B - V)$ . The measurement of  $\Delta m_{15}(B)$  is also highly sensitive to how well  $t_{\text{peak}}(B)$  is determined. By comparison, deriving  $s_0^*$  is simply measuring a slope, which does not require determining either of those two timings; instead,  $s_0^*$  can be determined for an SN which is not observed around peak brightness and/or lacks coverage at later times around  $t_{\text{max}}(B - V)$ .

#### 4. Measurement Procedure

In practice, when either  $t_{\text{peak}}(B)$  or  $t_{\text{max}}(B - V)$  is absent, it is not possible to use the phase range of  $([t_s = 0.3 t_{\text{max}}(B - V) - 2, t_e = 0.9 t_{\text{max}}(B - V)])$  with respect to  $t_{\text{peak}}(B)$  to fit  $s_0^*$ . Figure 5 shows light curves with different temporal coverages. Below we provide a practical procedure to measure  $s_0^*$  for such light curves.

1. If the B-band light curve around the peak is available to measure  $t_{\text{peak}}(B)$ , but there is no sufficiently late observation to determine the break time in the  $B - V$  color curve. First, start by fitting all data after  $t_{\text{peak}}(B)$  to get the initial  $s_0^*$ , and then use Equation (4) to estimate  $s_{BV}$  and subsequently  $t_{\text{max}}(B - V) = s_{BV} \times 30$  days. Then use the range of  $[0.3 t_{\text{max}}(B - V) - 2, 0.9 t_{\text{max}}(B - V)]$  for the next fitting and iteratively repeat this process until it converges. See the left column of Figure 5 for some examples in this category.
2. If the  $B - V$  color curve around the break time is available to measure the time of maximum  $B - V$  color, but there is no B-band coverage over the peak to measure  $t_{\text{peak}}(B)$ . In this case, without the reference time of  $t_{\text{peak}}(B)$ , a new reference time of  $t_{\text{break}}$  (measured as the time of maximum  $B - V$  color) will be used. First, start by fitting all data before  $t_{\text{break}}$  to get the initial  $s_0^*$ , and use Equation (4) to estimate  $t_{\text{max}}(B - V)$ . Then use the range from  $0.7 t_{\text{max}}(B - V) + 2$  to  $0.1 t_{\text{max}}(B - V)$  days before  $t_{\text{break}}$  for the next fitting and iteratively repeat this process until it converges. See the middle column of Figure 5 for some examples in this category.
3. If neither the B-band peak nor the break part in the  $B - V$  color curve is available. The value of  $s_0^*$  can be estimated by fitting the available color data that are consistent with

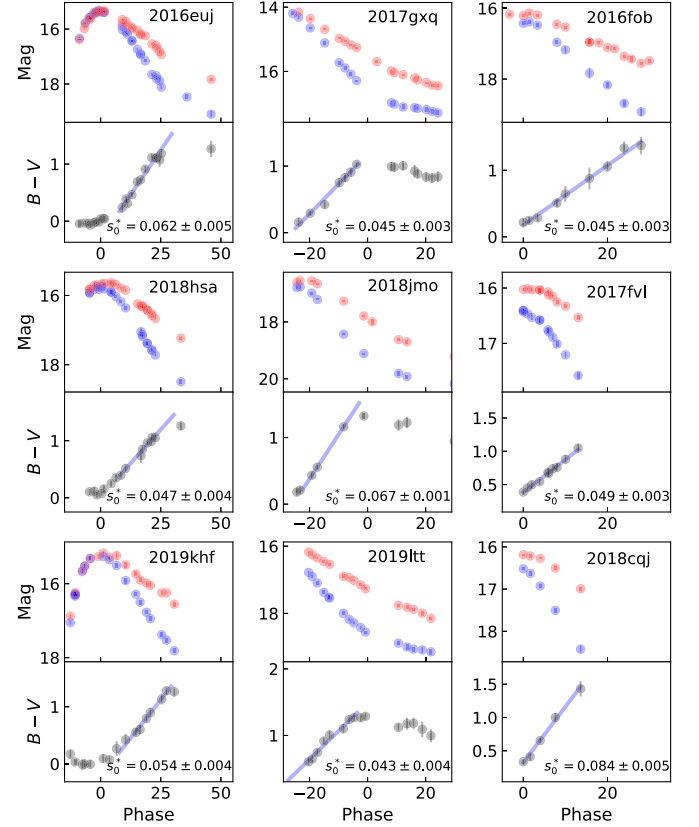


**Figure 5.** Examples of  $B$  and  $V$  light curves as well as  $B - V$  color curves with different temporal coverages as listed in Section 4. SNe Ia in the left column (SNe 2016euj, 2018hsa, and 2019khf) belong to the category that has the measurement of  $t_{\text{peak}}(B)$  but no  $t_{\text{max}}(B - V)$ , and the phase of these SNe is relative to  $t_{\text{peak}}(B)$ . SNe Ia in the middle column (SNe 2017gxq, 2018jmo, and 2019lft) have the time of the maximum  $B - V$  color ( $t_{\text{break}}$ ) but no  $t_{\text{peak}}(B)$ , and the phase of these SNe is relative to  $t_{\text{break}}$ . SNe Ia in the right column (SNe 2016fob, 2017fvl, and 2018ccj) have neither  $t_{\text{peak}}(B)$  nor  $t_{\text{max}}(B - V)$ , and the phase of these SNe is relative to the time of the first  $B - V$  data point. For each object, the upper plot shows the  $B$ -band (in blue color) and the  $V$ -band (in red color) light curves, and the lower plot displays the  $B - V$  color curve (black dots), the best-fit linear model (blue line), and the corresponding  $s_0^*(B - V)$ . The extent of the blue line indicates the range of data used to calculate the rising color slope according to the procedures in Section 4.

a straight line, but this may introduce systematic uncertainties owing to the uncharacterized fitting range. See the right column of Figure 5 for some examples in this category.

#### 5. Summary and Discussion

In summary, we find a linear relation between the color-stretch parameter ( $s_{BV}$ ) and the rising color slope ( $s_0^*(B - V)$ ) of the  $B - V$  color after the  $B$ -band peak, and this relation is applicable to the whole  $s_{BV}$  range of SNe Ia. With this linear relation,  $s_0^*(B - V)$  can be used to infer  $s_{BV}$ , which is known to be tightly correlated with the peak luminosity; in comparison, obtaining  $s_0^*(B - V)$  requires less demanding light-curve coverage than  $s_{BV}$ . What also distinguishes  $s_0^*(B - V)$  from  $\Delta m_{15}(B)$  and its variants (e.g.,  $\Delta m_8$ ,  $\Delta m_{30}$ ; Sharon & Kushnir 2022) is that measuring  $s_0^*(B - V)$  does not necessarily need coverage over the light-curve peak. Therefore, applying  $s_0^*(B - V)$  can broaden the capacity of estimating the peak luminosity, which is a key parameter of SNe Ia.

It will be interesting to study whether  $s_0^*$  measured in a color other than  $B - V$  has a similar correlation with  $s_{BV}$ . In a limited check we perform using the multiband light curves from the third photometry data release of the first stage of the Carnegie Supernova Project (CSP-I; Krisciunas et al. 2017), we find no good correlation between  $s_0^*(g - r)$  and  $s_{BV}$  (or  $s_{gr}$ ). The lack of a good correlation between  $s_0^*(g - r)$  and  $s_{BV}$  (or  $s_{gr}$ ) might be related to the emergence of secondary bumps in the  $r$ -band light curves of some SNe Ia starting  $\sim 15$  days after the  $B$ -band peak (see, e.g., Papadogiannakis et al. 2019).

Another future research direction is to study the underlying physical mechanism of the  $s_{BV} - s_0^*(B - V)$  relation, and it remains to be seen whether it can be interpreted by the same physical process for the WLR via  $s_{BV}$  (Wygoda et al. 2019) or some other aspect of SN physics.

As shown by Burns et al. (2014, 2018), the WLR via  $s_{BV}$  has been successfully used to accurately measure the Hubble constant. Owing to its correlation with  $s_{BV}$ ,  $s_0^*$  has the potential to be used for cosmology as an alternative proxy of light-curve width parameter, and since relatively sparse light curves are common for high- $z$  SNe Ia used in cosmological studies,  $s_0^*$  may be particularly promising because it is less demanding on light-curve coverage. Further investigations will be needed to establish whether  $s_0^*$  will be viable for precision cosmology.

We thank Chris Burns for discussing  $s_{BV}$  with us. We acknowledge the Telescope Access Program (TAP) funded by the NAOC, CAS, and the Special Fund for Astronomy from the Ministry of Finance. We acknowledge SUPA2019A (PI M. D. Stritzinger) via OPTICON. C.S.K., K.Z.S., and B.J.S. are supported by NSF grants AST-1515927, AST-1814440, and AST-1908570. M.D.S. acknowledges funding from the Villum Fonden (project numbers 13261 and 28021), and also a project grant (8021-00170B) from the Independent Research Fund Denmark. N.E.R. acknowledges partial support from MIUR, PRIN 2017 (grant 20179ZF5KS), and the Spanish MICINN grant PID2019-108709GB-I00 and FEDER funds. A.V.F.'s supernova group is grateful for financial assistance from the Christopher R. Redlich Fund, the Miller Institute for Basic Research in Science (U.C. Berkeley; A.V.F. was a Miller Senior Fellow), and many individual donors. J.L.P. is supported in part by FONDECYT through grant 1191038 and by the Ministry of Economy, Development, and Tourism's Millennium Science Initiative through grant IC120009, awarded to The Millennium Institute of Astrophysics, MAS. B.J.S. is also supported by NSF grants AST-1920392 and AST-1911074. M.G. is supported by the Polish NCN MAESTRO grant 2014/14/A/ST9/00121. Polish participation in SALT is funded by grant MNiSW DIR/WK/2016/07. S.M.H. is supported by the Natural Science Foundation of Shandong province (#JQ201702), and the Young Scholars Program of Shandong University (#20820162003). Support for T.W.-S.H. was provided by NASA through the NASA Hubble Fellowship grant #HST-HF2-51458.001-A awarded by the Space Telescope Science Institute, which is operated by the Association of Universities for Research in Astronomy, Inc., for NASA, under contract NAS5-26555. Research at Lick Observatory is partially supported by a generous gift from Google. We thank the staffs of the various observatories at which data were obtained for their excellent assistance.

*Software:* Kapteyn (Terlouw & Vogelaar 2016), Astropy (Astropy Collaboration et al. 2018), matplotlib (Caswell et al. 2021).

## ORCID iDs

Ping Chen  <https://orcid.org/0000-0003-0853-6427>  
 Subo Dong  <https://orcid.org/0000-0002-1027-0990>  
 Chris Ashall  <https://orcid.org/0000-0002-5221-7557>  
 D. Bersier  <https://orcid.org/0000-0001-7485-3020>  
 S. Bose  <https://orcid.org/0000-0003-3529-3854>  
 Thomas G. Brink  <https://orcid.org/0000-0001-5955-2502>  
 Enrico Cappellaro  <https://orcid.org/0000-0001-5008-8619>  
 N. Elias-Rosa  <https://orcid.org/0000-0002-1381-9125>  
 Alexei V. Filippenko  <https://orcid.org/0000-0003-3460-0103>  
 Mariusz Gromadzki  <https://orcid.org/0000-0002-1650-1518>  
 Thomas W.-S. Holoien  <https://orcid.org/0000-0001-9206-3460>  
 C. S. Kochanek  <https://orcid.org/0000-0001-6017-2961>  
 P. Lundqvist  <https://orcid.org/0000-0002-3664-8082>  
 Peter A. Milne  <https://orcid.org/0000-0002-0370-157X>  
 J. A. Muñoz  <https://orcid.org/0000-0001-9833-2959>  
 Robert Mutel  <https://orcid.org/0000-0003-1511-6279>  
 A. Pastorello  <https://orcid.org/0000-0002-7259-4624>  
 Simon Prentice  <https://orcid.org/0000-0003-0486-6242>  
 J. L. Prieto  <https://orcid.org/0000-0003-0943-0026>  
 B. J. Shappee  <https://orcid.org/0000-0003-4631-1149>  
 M. D. Stritzinger  <https://orcid.org/0000-0002-5571-1833>  
 Todd A. Thompson  <https://orcid.org/0000-0003-2377-9574>  
 Lina Tomasella  <https://orcid.org/0000-0002-3697-2616>  
 Steven Villanueva  <https://orcid.org/0000-0001-6213-8804>

## References

- Ashall, C., Lu, J., Burns, C., et al. 2020, *ApJL*, **895**, L3  
 Astropy Collaboration, Price-Whelan, A. M., & Sipőcz, B. M. 2018, *AJ*, **156**, 123  
 Boggs, P. T., Byrd, R. H., & Schnabel, R. B. 1987, *SIAM J. Sci. Stat. Comput.*, **8**, 1052  
 Boisseau, J. R., & Wheeler, J. C. 1991, *AJ*, **101**, 1281  
 Burns, C. R., Parent, E., Phillips, M. M., et al. 2018, *ApJ*, **869**, 56  
 Burns, C. R., Stritzinger, M., Phillips, M. M., et al. 2011, *AJ*, **141**, 19  
 Burns, C. R., Stritzinger, M., Phillips, M. M., et al. 2014, *ApJ*, **789**, 32  
 Caswell, T. A., Droettboom, M., Lee, A., et al. 2021, matplotlib/matplotlib: REL: v3.3.4, Zenodo, doi:10.5281/zenodo.4475376  
 Chen, P., Dong, S., Kochanek, C. S., et al. 2022, *ApJS*, **259**, 53  
 Conley, A., Goldhaber, G., Wang, L., et al. 2006, *ApJ*, **644**, 1  
 Filippenko, A. V., Richmond, M. W., Branch, D., et al. 1992a, *AJ*, **104**, 1543  
 Filippenko, A. V., Richmond, M. W., Matheson, T., et al. 1992b, *ApJL*, **384**, L15  
 Gall, C., Stritzinger, M. D., Ashall, C., et al. 2018, *A&A*, **611**, A58  
 Guy, J., Astier, P., Baumont, S., et al. 2007, *A&A*, **466**, 11  
 Hamuy, M., Phillips, M. M., Maza, J., et al. 1995, *AJ*, **109**, 1  
 Hamuy, M., Phillips, M. M., Suntzeff, N. B., et al. 1996, *AJ*, **112**, 2438  
 Hoeflich, P., Hsiao, E. Y., Ashall, C., et al. 2017, *ApJ*, **846**, 58  
 Jha, S., Riess, A. G., & Kirshner, R. P. 2007, *ApJ*, **659**, 122  
 Krisciunas, K., Contreras, C., Burns, C. R., et al. 2017, *AJ*, **154**, 211  
 Leibundgut, B., Kirshner, R. P., Phillips, M. M., et al. 1993, *AJ*, **105**, 301  
 Papadogiannakis, S., Dhawan, S., Morosin, R., & Goobar, A. 2019, *MNRAS*, **485**, 2343  
 Perlmutter, S. A., Deustua, S., Gabi, S., et al. 1997, in Proc. NATO Advanced Study Institute 486, Thermonuclear Supernovae, ed. P. Ruiz-Lapuente, R. Canal, & J. Isern (Dordrecht: Springer), 749  
 Phillips, M. M. 1993, *ApJL*, **413**, L105  
 Phillips, M. M., & Burns, C. R. 2017, in Handbook of Supernovae, ed. A. W. Alsabti & P. Murdin (Cham: Springer), 2543  
 Phillips, M. M., Wells, L. A., Suntzeff, N. B., et al. 1992, *AJ*, **103**, 1632  
 Prieto, J. L., Rest, A., & Suntzeff, N. B. 2006, *ApJ*, **647**, 501  
 Pskovskii, I. P. 1977, *SvA*, **21**, 675  
 Pskovskii, Y. P. 1984, *SvA*, **28**, 658  
 Riess, A. G., Press, W. H., & Kirshner, R. P. 1996, *ApJ*, **473**, 88  
 Ruiz-Lapuente, P., Cappellaro, E., Turatto, M., et al. 1992, *ApJL*, **387**, L33  
 Sharon, A., & Kushnir, D. 2022, *MNRAS*, **509**, 5275

Terlouw, J. P., & Vogelaar, M. G. R. 2016, Kapteyn Package: Tools for Developing  
Astronomical Applications, Astrophysics Source Code Library, ascl:[1611.010](#)  
Turatto, M., Benetti, S., Cappellaro, E., et al. 1996, [MNRAS](#), **283**, 1

Wang, L., Goldhaber, G., Aldering, G., & Perlmutter, S. 2003, [ApJ](#), **590**, 944  
Wang, L., Strovink, M., Conley, A., et al. 2006, [ApJ](#), **641**, 50  
Wygoda, N., Elbaz, Y., & Katz, B. 2019, [MNRAS](#), **484**, 3941